2023 IEEE/ASME International Conference on Advanced Intelligent Mechatronics (AIM)
June 28-30, 2023. Seattle, Washington, USA

Parameter identification related to vertical dynamic of a self-stabilizing monorail vehicle

Martin Griese*, Seyed Davood Mousavi† and Thomas Schulte‡
Institute for Energy Research (iFE)
Ostwestfalen-Lippe University of Applied Sciences and Arts
32657 Lemgo, Germany
Email: *martin.griese@th-owl.de, †seyed.mousavi@th-owl.de, ‡thomas.schulte@th-owl.de

***Abstract*—Currently, numerous single-track railway lines are disused due to economic reasons. However, one way they could be reactivated for a bidirectional on-demand service traffic by small vehicles that use only one rail. MONOCABs are such small cabin-like vehicles, stabilized by a system of control moment gyroscopes and a trim mass. They could make an important contribution to improve the mobility offer especially in rural areas. Regarding the MONOCAB, there is currently no reference in comparison with other vehicles. It is mandatory to gain experience before transferring such a new vehicle concept into commercial operation. Especially the safe and robust commissioning of the stabilization control system is crucial and therefore requires an elaborated procedure. At this step, parameters related to the vertical dynamics have to be determined beforehand. This paper presents a comparative investigation of methods to estimate the moment of inertia and gravitational torque constant. Multiple methods in time-domain and frequency-domain are experimentally evaluated and compared with each other. Experimental tests are carried out with a full-scale monorail vehicle.**

***Index Terms*—Parameter identification, Vehicle dynamics, Control moment gyroscope, Roll stabilization, Monorail vehicles**

I. Introduction

The expansion and renovation of existing railway lines are essential parts to make transport policies more climate friendly. This also includes the reactivation of disused single-track sections. In Germany, the total length of such disused tracks is about 5000 km. An appropriate reactivation concept could be based on small autonomously driving monorail vehicles - MONOCABs. MONOCABs are narrow vehicles which use one rail only. This vehicle enables a demand oriented bidirectional traffic on conventional single-track routes without causing high personnel and investment costs. By using MONOCABs, a flexible and economically as well as ecologically efficient connection from rural areas to medium-sized centers could be established, for example. The research project MONOCAB OWL aims to prove the feasibility of the MONOCAB concept. Two full-scale experimental vehicles are developed, constructed and finally tested on a real disused track.

MONOCABs are intended to use conventional railways without an additional mechanical support. This requires that the vehicle stabilizes itself on the rail by control moment gyroscopes (CMGs). Such kind of gyro stabilized vehicles were firstly developed by Louis Brennan who successfully demonstrated a monorail vehicle with a weight of 22 tonnes, [1]. Other gyro-stabilized vehicles have been developed at about the same time, [2], [3]. However, a commercial implementation did not occur presumably due to technical problems (e.g. lack of fail-safe behavior) and a lack of appropriate commercial applications in the time of early mass mobility.

Beside the previous mentioned monorail vehicles, similar stabilization and motion control techniques are also discussed in aerospace applications [4], boats and yachts [5], motor- and bicycles [6]–[11] as well as for medical purposes [12]. A comprehensive review of stabilization applications (land, sea and spacecraft) and techniques as well as modeling and control strategies can be found in [9] and [13]. Different solutions for the stabilization and control of such vehicles have been investigated. However, the combination of CMGs with a trim mass is of particular interest in this project which has not been discussed to full extent in literature.

The system and control design of stabilization systems is a complex task. A well-known approach is the model-based design which allows analytical calculations as well as numerical simulations. However, in case of sensitive controller or unkown model parameters an elaborated commissioning concept is important. The contribution of this paper is the presentation and comparison of parameter identification procedures as part of the commissioning process of the MONOCAB stabilization system. Model parameters especially mechanical properties such as masses and inertias can usually only be roughly estimated, e.g. from CAD data. By experimental identification methods, parameter values can be estimated more precisely. The paper is structured as follows: An overview on the stabilization system and controller is given in section II. Section III describes the identification procedures which are experimentally investigated and compared to each other in section IV.

II. System overview and modeling

As mentioned above, the MONOCAB needs a stabilization system to control the rolling motion. A combination of multiple systems is required as illustrated by figure 1a). Figure 1b) describes the mechanical quantities which are further on used.

The primary system consists of control moment gyroscopes (CMGs) that provide the basic vertical stabilization and compensate dynamic disturbances. A CMG consists of a flywheel

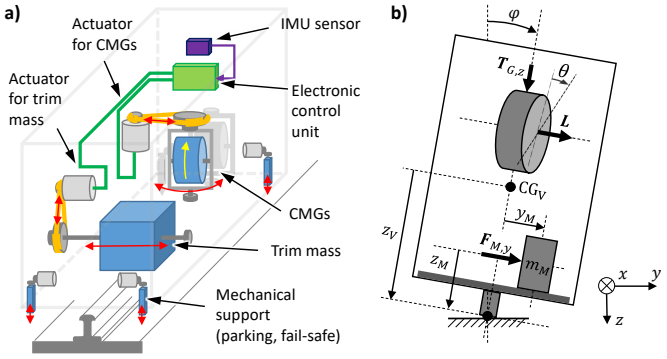

Fig. 1. Schematic representation of the stabilization system.

in a gimbal rotating at a high spinning speed $\omega_{G,y}$. The relevant angular momentum of each flywheel is described by $L = I_{G,yy} \cdot \omega_{G,y}$. The gimbal allows a precession motion as an additional rotational degree of freedom, further on described by the angle θ. In order to control this motion, an inverter-fed electrical drive is considered. The actuation torque $T_{G,z}$ yields an acceleration of the gimbal (inertia $I_{G,zz}$) with respect to their vertical axis z. Due to the fact that the precession torque of CMGs is proportional to the precession speed and limited to the range $-90° < \theta < 90°$, they are not capable of compensating stationary disturbances. For this purpose, a trim mass m_M can be actively moved by an inverter-fed motor (force $F_{M,y}$) in lateral direction (y) of the vehicle. The lateral displacement y_M yields a desired gravitational torque to compensate stationary disturbances. This is further on named as stationary stabilization system. For parking and in case of emergencies, the MONOCAB has mechanical support systems that allows the vehicle to rest on the track bed. This is named as tertiary stabilization system. More details about the stabilization concept can be found in [14].

For simulation and control design, we derived a physical-based model of the vertical dynamics of the MONOCAB via the Lagrangian approach, [15]. The model is nonlinear and mainly used for detailed simulations. Considering an active stabilization system, a linearization of the model is reasonable, as the roll angle φ remains in valid operation range. In our previous work [15], [16], a detailed comparison between linear and non-linear model was performed and it was shown that in realistic operating points the differences between both models are very small and negligible. Therefore in this paper the linear model is further on used for parameter identification without losing accuracy.

Underlying the stabilization control, a speed control for both actuators is implemented. The resulting state-space model ($\dot{\mathbf{x}} = \mathbf{A}\cdot\mathbf{x}+\mathbf{B}\cdot\mathbf{u}$, $\mathbf{y} = \mathbf{C}\cdot\mathbf{x}$) with $\mathbf{x} = \begin{bmatrix} \varphi & \dot{\varphi} & y_M & \dot{y}_M & \theta & \dot{\theta} \end{bmatrix}^T$, $\mathbf{u} = \begin{bmatrix} \dot{y}_M^* & \dot{\theta}^* \end{bmatrix}^T$ and $\mathbf{y} = \begin{bmatrix} \varphi & \theta \end{bmatrix}^T$ is described by the matrices in (1). Here, $\tilde{I}_{V,xx}$, m_V and $z_V < 0$ are the inertia, mass and center of gravity (height) of the total vehicle and $\tau_{\sigma,G}$ as well as $\tau_{\sigma,M}$ are the total sum of the small time constants considering the speed controls of the CMGs and trim mass. The quantities $\dot{y}_M^*$ and $\dot{\theta}^*$ are the set-point values for the speed control the trim mass and CMGs.

$$\mathbf{A} = \begin{bmatrix} 0 & 1 & 0 & 0 & 0 & 0 \\ \frac{-m_V \cdot z_V \cdot g}{\tilde{I}_{V,xx}} & 0 & \frac{m_m \cdot g}{\tilde{I}_{V,xx}} & \frac{-z_M \cdot m_M}{4 \cdot \tau_{\sigma,M} \cdot \tilde{I}_{V,xx}} & 0 & \frac{L}{\tilde{I}_{V,xx}} \\ 0 & 0 & 0 & 1 & 0 & 0 \\ 0 & 0 & 0 & \frac{-1}{4 \cdot \tau_{\sigma,M}} & 0 & 0 \\ 0 & 0 & 0 & 0 & 0 & 1 \\ 0 & 0 & 0 & 0 & 0 & \frac{-1}{4 \cdot \tau_{\sigma,G}} \end{bmatrix} \quad (1)$$

$$\mathbf{B} = \begin{bmatrix} 0 & 0 \\ \frac{z_M \cdot m_M}{4 \cdot \tau_{\sigma,M} \cdot \tilde{I}_{V,xx}} & 0 \\ 0 & 0 \\ \frac{1}{4 \cdot \tau_{\sigma,M}} & 0 \\ 0 & 0 \\ 0 & \frac{1}{4 \cdot \tau_{\sigma,G}} \end{bmatrix} \quad \mathbf{C} = \begin{bmatrix} 1 & 0 & 0 & 0 & 0 & 0 \\ 0 & 0 & 0 & 0 & 1 & 0 \end{bmatrix}$$

By analytical calculations considering a limited dynamic of the speed control of the CMGs, it can be shown that the relevant inertia of the roll motion $\tilde{I}_{V,xx}$ is higher than the real mechanical inertia $I_{V,xx}$ of the system. This occurs due to the physical coupling between the precession motion of the CMGs and the roll motion of the vehicle. Depending on the dynamic of the speed control ($\tau_{\sigma,G}$), the relevant inertia can be evaluated by $\tilde{I}_{V,xx} \approx I_{V,xx} + 8 \cdot \tau_{\sigma,G}^2 \cdot L^2 / I_{G,zz}$. In the ideal case ($\tau_{\sigma,G} = 0$), the real mechanical inertia is obtained.

Based on the plant model in (1), a state feedback control is designed as linear quadratic integral regulators (LQI) to provide the nominal stabilization function. This variant uses both actuators and is described in a previous paper [16].

However, in order to provide a suitable test signal for parameter identification and first commissioning, experiences on the real system have shown that a simpler control concept with less parameters is useful. Assuming that the trim mass is fixed in its neutral position meaning the vehicle is statically balanced at $\varphi = 0°$, the trim mass can be analytically removed out of the plant model in (1). Without the trim mass, the controllability of the precession angle θ is not fulfilled. This state can be simplified removed, because no feedback of θ is included in the full linear model. The reduced model is described by $\dot{\mathbf{x}}_R = \mathbf{A}_R \cdot \mathbf{x}_R + \mathbf{B}_R \cdot u_R$, $y_R = \mathbf{C}_R \cdot \mathbf{x}_R$ with $\mathbf{x}_R = \begin{bmatrix} \varphi & \dot{\varphi} & \dot{\theta} \end{bmatrix}^T$, $u_R = \dot{\theta}^*$, $y_R = \varphi$ and (2).

$$\mathbf{A}_R = \begin{bmatrix} 0 & 1 & 0 \\ \frac{-m_V \cdot z_V \cdot g}{\tilde{I}_{V,xx}} & 0 & \frac{L}{\tilde{I}_{V,xx}} \\ 0 & 0 & \frac{-1}{4 \cdot \tau_{\sigma,G}} \end{bmatrix} \quad (2)$$

$$\mathbf{B}_R = \begin{bmatrix} 0 \\ 0 \\ \frac{1}{4 \cdot \tau_{\sigma,G}} \end{bmatrix} \quad \mathbf{C}_R = \begin{bmatrix} 1 & 0 & 0 \end{bmatrix}$$

A state feedback control designed as linear quadratic integral regulators (LQI) is developed based on this reduced plant model (2) similar to the nominal stabilization controller, see [16]. Compared to the full model and control, this variant is of significant lower order and has less parameters. Hence, it is more suitable for parameter identifications and first commissioning steps. However, it is not usable for a nominal operation of the vehicle due to the fact that the precession angle θ of the

CMGs is not controlled. Low stationary disturbances cause a slow drift of the gyro precession until mechanical limits or $\theta = 90°$ is reached.

The mechanical parameters in (1) and (2) which are unknown and need to be identified are the inertia $I_{V,xx}$, the total vehicle mass m_V and the center of gravity (height) z_V. Using the speed controlled CMGs, the system can be excited and the unknown parameters can be estimated. Due to the fact that the precession speed $\dot{\theta}$ is approximately proportional to the precession torque $T_{G,x}$, a simple relationship can be derived from (2) as described by the following transfer function:

$$G(s) = \frac{\varphi(s)}{T_{G,x}(s)} = \frac{1}{I_{V,xx} \cdot s^2 - T_V}, \tag{3}$$

where $T_{G,x}$ is defined as $T_{G,x} = L \cdot \dot{\theta}$ and T_V describes the gravitational torque and is defined as $T_V = m_V \cdot z_V \cdot g$. The individual parameters (m_V, z_V) shall not be estimated as only the gravitational torque as summarized parameter is relevant for the control design.

III. Identification procedures

A. Time domain - Minimization of the output error

This section discusses identification via nonlinear optimization of the output error which is perhaps the most obvious possibility in the time domain, especially with the computers available today that provide methods for nonlinear optimization and also have sufficient computing power [17].

All methods for parameter estimation require suitable test data, in particular an excitation of the relevant variables. The following test procedure was used for the methods in time domain: The vehicle rests on the tertiary stabilization (see section II) in a slightly tilted position with maximum roll angle $\varphi = 4°$. Then a step-wise change of the precession speed $\dot{\theta}$ respectively torque $T_{G,x}$ is applied until the vehicle reaches its vertical position ($\varphi = 0°$).

On the one hand, the roll angle $\hat{\varphi}(t)$ can be simulated considering the existing model (3), on the other hand, it can be estimated using the sensor data and the Kalman filter $\tilde{\varphi}(t)$, [18]. By this method, the parameter vector is adjusted so that the deviation between the estimated output and simulated output $\tilde{e}(t) = \tilde{\varphi}(t) - \hat{\varphi}(t)$ is minimized. For a minimum square distance, this corresponds to the performance function

$$P(\rho) = \sum_{k=0}^{N-1} \left(\hat{\varphi}(t_k, \rho) - \tilde{\varphi}(t)\right)^2, \tag{4}$$

where N is the number of measurement points.

The simplex search method of Lagarias et al. [19] is applied as optimization algorithm to minimize the defined performance function and estimate the parameter vector ρ

$$\hat{\rho} = \arg \underbrace{\min}_{\rho} P(\rho). \tag{5}$$

In general, it cannot be guaranteed that such numerical methods will find a global optimum in a non-linear optimization problem. We assume that the existing problem is convex due to the fact that an equal parameter vector was estimated by an empirical variation of the initial parameter values.

B. Time domain - Least squares method

To apply the linear LS method, the relationship must be written in a linear form with respect to the parameters [17]. For each of the 2 parameters, there is an input variable, denoted here as $\psi_{j,k}$, where $j = 1, 2$ and $k = 1, \cdots, N$ and N is the number of measurement points. It is therefore necessary to distinguish between the physical inputs $T_{G,x,k}$ and the input variables $\psi_{j,k}$ of the LS problem. It is also useful to distinguish between the physical output and the output variable y_k of the LS problem.

Therefore, the considered relationship can be expressed in the form $y_k = \theta_1 \psi_{1,k} + \theta_2 \psi_{2,k}$. Considering (3) in time domain, the input variables and the parameters are summarized to an input vector and a parameter vector, respectively

$$\begin{aligned} \boldsymbol{\psi}_k^T &= \begin{bmatrix} \psi_{1,k} & \psi_{2,k} \end{bmatrix} = \begin{bmatrix} \ddot{\tilde{\varphi}}_k & -\tilde{\varphi}_k \end{bmatrix} \\ \boldsymbol{\theta} &= \begin{bmatrix} \theta_1 & \theta_2 \end{bmatrix}^T = \begin{bmatrix} I_{V,xx} & T_V \end{bmatrix}^T \end{aligned} \tag{6}$$

The output vector of the LS problem is equal to physical input vector $y_k = T_{G,x,k} = \boldsymbol{\psi}_k^T \boldsymbol{\theta}$. To solve the LS problem, the same input and measurement data are used as in section III-A, but $\ddot{\tilde{\varphi}}_k$ is not measurable and since $\dot{\tilde{\varphi}}_k$ is noisy, its derivative easily covers the actual useful signal. Therefore, an approach that provides some filtering is necessary.

In this case a state variable filter is used. The idea of the state variable filter is based on the use of a filter like Butterwoth with angular frequency ω represented in the form

$$\begin{aligned} \begin{bmatrix} \ddot{\tilde{\varphi}}_F \\ \tilde{\varphi}_F^{(3)} \end{bmatrix} &= \begin{bmatrix} 0 & 1 \\ -\omega^2 & -\sqrt{2}\omega \end{bmatrix} \begin{bmatrix} \dot{\tilde{\varphi}}_F \\ \ddot{\tilde{\varphi}}_F \end{bmatrix} + \begin{bmatrix} 0 \\ \omega^2 \end{bmatrix} \dot{\tilde{\varphi}} \\ \ddot{\tilde{\varphi}}_F &= \begin{bmatrix} 0 & 1 \end{bmatrix} \begin{bmatrix} \dot{\tilde{\varphi}}_F \\ \ddot{\tilde{\varphi}}_F \end{bmatrix}, \end{aligned} \tag{7}$$

where $\dot{\tilde{\varphi}}$ is the filter input and $\dot{\tilde{\varphi}}_F$ is the filter output. In this form the second filter state corresponds to the first derivative $\ddot{\tilde{\varphi}}_F$ of the filtered signal.

After this filtering, the input vector can be actualized and the parameter vector can be estimated based on the LS problem $\hat{\boldsymbol{\theta}} = \left(\boldsymbol{\Psi}^T \boldsymbol{\Psi}\right)^{-1} \boldsymbol{\Psi}^T \boldsymbol{\theta} \boldsymbol{y}$. By using this method, it is assumed that the input and output of LS problem can be measured accurately.

C. Frequency domain - Minimization of the output error

This section and the following describes procedures which uses the frequency response of the system. As basis for both algorithms, the numerical frequency response of the system (3) need to be experimentally estimated [17]. In order to excite the system in the relevant vertical position ($\varphi = 0°$), a test signal can be superimposed during active stabilization control (see section II). Compared to the previous time domain methods, these procedures are more complex and require a proper stabilization control system. In this contribution, these methods are included for comparison and validation but may not be practical in a real application.

However, there are two variants conceivable as test excitation. First, a sine sweep can be implemented as an offset to the set value of the stabilization control (roll angle φ). Especially the lower frequency range and therefore the effect of the graviational torque can be estimated well but the frequency range that can be determined is limited due to the controller dynamics. As second variant, an excitation could be implemented as an offset to the control output $\dot{\theta}^*$. This allows an excitation of a higher frequency range, but the lower frequency range is not estimated reliably due to the fact that the superimposed control dampens the vehicle movement.

In this contribution, we use the first variant and choose a sine sweep with frequencies between 0 and 10 Hz. The bandwidth of the overall stabilization control is limited to about 8 Hz. Therefore, an excitation with a higher frequency is not reasonable. The recorded measurement data is analyzed offline by the method of Welch [20] in order to estimate the frequency response $\tilde{G}(j\omega)$. The captured data is divided into K subsequences and afterwards transferred into frequency domain using Hanning windows. The estimated transfer function is obtained by the division of the cross- and auto power spectral densities $\tilde{S}_{xy}^{W}(j\omega)$ resp. $\tilde{S}_{xx}^{W}(j\omega)$ by

$$\tilde{G}(j\omega) = \frac{\tilde{S}_{xy}^{W}(j\omega)}{\tilde{S}_{xx}^{W}(j\omega)} = \frac{\sum_{i=1}^{K} \tilde{S}_{xy,i}(j\omega)}{\sum_{i=1}^{K} \tilde{S}_{xx,i}(j\omega)} \tag{8}$$

in which the spectral densities $\tilde{S}_{xy}(j\omega)$ and $\tilde{S}_{xx}(j\omega)$ are calculated by FFT from the corresponding correlation functions. In this application, the estimated precession torque $T_{G,x}$ serves as input $x(t)$ while the measured roll angle φ is chosen as output $y(t)$. By comparing the numerical results ($\tilde{G}(j\omega_l)$) with the modeled behavior ($\hat{G}(j\omega_l, \rho)$), the unknown parameters ρ can be estimated. In this paper only the amplitude responses are considered for the following performance function

$$P(\rho) = \sum_{l=1}^{N} \left(\left| \hat{G}(j\omega_l, \rho) \right| - \left| \tilde{G}(j\omega_l) \right| \right)^2, \tag{9}$$

where N is the number of estimated frequency points. Similar to section III-A, the simplex search method is applied.

D. Frequency domain - Minimization of the equation error

Based on the frequency domain data (see previous subsection), a further method is conceivable for this application [21]. For this purpose, (3) is used and reparameterized with n_0 and d_2 and the frequency response is given in the following form

$$\hat{G}(\omega) = \frac{1}{I_{V,xx}(j\omega)^2 - T_V} = \frac{n_0}{d_2(j\omega)^2 + 1} = \frac{\hat{N}(j\omega)}{\hat{D}(j\omega)}. \tag{10}$$

From modeled frequency response (10) and measured frequency response $\tilde{G}(j\omega_l)$, equation error is given as follows

$$\hat{e}_l = \tilde{G}(j\omega_l) - \underbrace{((1 - \hat{D}(j\omega_l))\tilde{G}(j\omega_l) + \hat{N}(j\omega_l))}_{\tilde{G}'(j\omega_l)}, \tag{11}$$

where $l = 1, \cdots, N$ and N is the number of measurement points. The goal is to minimize the sum of the squared errors, where a weight w_l is also provided for the individual errors. It applies $|\hat{e}_l|^2 = \hat{e}_l \hat{e}_l^*$, where $\hat{e}_l^*$ denotes the conjugate complex value of $\hat{e}_l$. This further gives $\hat{e}_l = \hat{e}_{R,l} + j\hat{e}_{I,l}$ with real values $\hat{e}_{R,l}$ and $\hat{e}_{I,l}$ and the performance function can also be written as

$$P = \sum_{l=1}^{N} \omega_l (\hat{e}_{R,l}^2 + \hat{e}_{I,l}^2) = \hat{e}^T W \hat{e}, \tag{12}$$

$2N$ equations are obtained, but no further complex variables appear. With the frequency response (10), the equation error (11) can be specified as

$$\begin{aligned} \hat{e}_l &= \tilde{G}(\omega_l) + \hat{d}_2 \tilde{G}(\omega_l)(j\omega_l)^2 - \hat{n}_0 \\ &= y_l - \boldsymbol{\psi}_l^T \hat{\boldsymbol{\theta}}, \end{aligned}$$

where $y_l = \tilde{G}(\omega_l)$ is the output, $\boldsymbol{\psi}_l^T = \begin{bmatrix} -\tilde{G}(\omega_l)(j\omega_l)^2 & 1 \end{bmatrix}$ is the input, and $\hat{\boldsymbol{\theta}} = \begin{bmatrix} d_2 & n_0 \end{bmatrix}^T$ is parameter vector of this LS problem.

The error $\hat{e}_l$ is separated into real and imaginary part and consequently the solution of the described weighted LS problem is $\hat{\boldsymbol{\theta}} = (\boldsymbol{\Psi}^T \boldsymbol{W} \boldsymbol{\Psi})^{-1} \boldsymbol{\Psi}^T \boldsymbol{W} \boldsymbol{y}$. The relative uncertainty increases with increasing frequency, and errors belonging to higher frequencies are much more strongly included in the total error due to the exponentiations of the frequency in the input vector. To counteract this effect, the inverse of the squared relative error are used as weights:

$$w_l = \left(\frac{\left| \tilde{G}(\omega_l) \right|}{\left| \Delta \tilde{G}(\omega_l) \right|} \right)^2. \tag{13}$$

IV. Experimental setup and results

In order to gain experience with the described identification procedures, an experimental test setup was realized and measurements were conducted. A first version of the MONOCAB as experimental vehicle has been realized in full scale where figure 2a) shows a CAD drawing of the technical substructure on which the passenger cabin is mounted. The substructure is based on a simple steel frame structure in which all required technical components (supply, communication, driving and stabilization systems) are installed.

As CMGs, two modified gyros MC² X5 DC of QUICK SPA provide a total angular momentum of $L \approx 3300 Nms$. The actuator concept for the precession movement is self developed and consists mainly of an inverter-fed bevel gear motor with a chain drive. The trim mass has a total weight of about $m_M \approx 500kg$ and is realized in a compact design via lead plates. The actuator concept for the trim mass is based on a ball screw drive and an inverter-fed motor. The vertical stabilization requires a measurement of the roll angle φ of the vehicle. For this purpose, the inertial measurement unit LPMS-IG1 of LP-RESEARCH provide raw data from its internal acceleration and gyro sensors. The roll angle φ is dynamically correct estimated by an implemented kalman filter, [16].

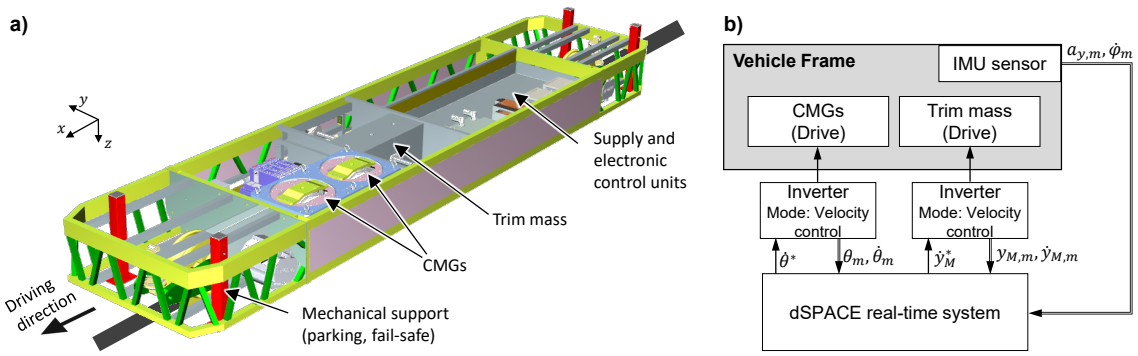

Fig. 2. Experimental test setup (a) and schematic diagram of the controlling and data capturing system (b).

The overall concept for controlling and data capturing is shown in figure 2b). As inverters for the stabilization actuators, we use servo amplifiers COMBIVERT S6 of KEB. For both actuators, first of all a speed control is implemented and commissioned using the inverters. The stabilization control concept and test excitation are implemented on the real-time system MicroAutobox 2 of dSPACE, also used for data capturing of the measured values. The data communication between the sensors, inverters and control units is realized via CAN communication networks. Before this real experiment, the setup and communication networks have been tested in offline and Hardware-in-the-Loop simulations, [16]. It was shown that communication latencies and cycle times do not have a dominant influence on the control.

The system is actuated with several inputs and, using the methods described in chapter III, the moment of inertia and the gravitational moment are estimated from measured data and presented in figure 3. In figure 3 the estimated parameters for each individual method are shown with smaller markings and their mean value with large markings. The mean values of large markings are shown as reference values with dashed lines. As can be seen, the standard deviation of the estimated values in the individual methods is not large, but except for output minimization error, the deviation from the reference values must be taken into account in the other 3 methods. Beside these experimental identified parameters, a first estimation of the mechanical properties was obtained by CAD calculation, also shown in figure 3. The CAD model does not include all details of the realized system (e.g. cables and smaller components) which explains the differences between the methods. In particular the gravitational torque is lower due to missing components in the CAD model.

By experimental consideration it is noticed that considered model in (3) contains a small error and this error was corrected by adding a static torque. Both methods in time domain are simply developed with corrected model and results are shown in figure 3 but in frequency domain due to caused non-linearity the model cannot be represented in form of transfer function and therefore this correction in model building is neglected. This approximation justifies the deviations of the estimated parameters in the frequency domain.

In time domain the method of output error minimization

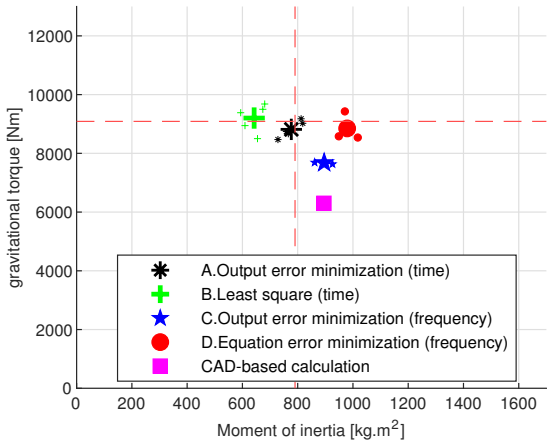

Fig. 3. Comparison between different methods in time and frequency domain.

shows a good result but despite the mentioned correction in LS method a deviation with reference values is visible. In section III-B the inputs of LS problem are assumed to be ideal measurable variables but $\ddot{\tilde{\varphi}}_F$ is derived from $\dot{\tilde{\varphi}}$ by state-variable filter. When using LS method, it is assumed that five classical Markov conditions [22] are satisfied. In the derived $\ddot{\tilde{\varphi}}_F$, however, the superimposed noise is not zero mean and therefore Markov conditions are violated and LS method is no longer consistent.

In order to validate and test the results of the procedures, the full stabilization control is parameterized using the mean values (dashed lines in figure 3) and various dynamic and static disturbances were tested. Figure 4 shows measurement and simulation results that demonstrate the disturbance response of the active stabilization control. For the simulation, the linear model (3) in combination with the same stabilization control was used. At about 1 second, one person sits on the edge of the steel frame which is roughly a disturbance of 550 Nm. For the simulation, the disturbance is modeled as a ramp-wise change from 0 to 550 Nm. Considering the roll angle φ, only a slight deviation below $0.05°$ can be noticed which confirms the good parameterization and is verified by the simulation. The second subplot shows that a precession movement occurs which compensates the dynamic disturbance. In this scenario, the angle θ is below $15°$ and thus has a high control reserve.

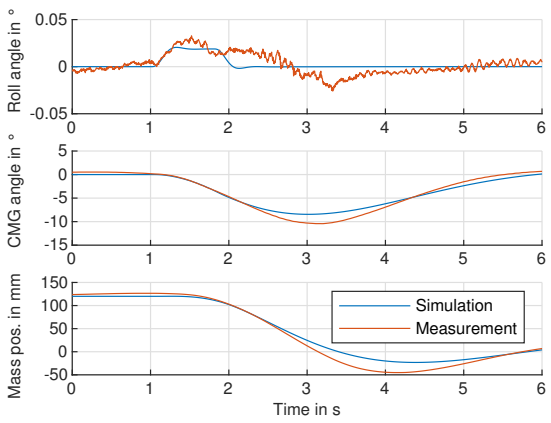

Fig. 4. Experimentally measured disturbance response of the stabilization system.

The trim mass provides the stationary balance which position is shown in the lower subplot. Here, a significant overshoot can be noticed at about 4 seconds. This is intended and necessary for resetting the CMG's precession angle to $\theta = 0°$. Comparing the results of the measurement with the simulation, slight differences can be noticed. They can be explained by non-modeled friction effects and delays. The experimental vehicle is mechanically protected by a safety catch which unintentionally also introduces friction with respect to the roll motion of the vehicle. The measurements show a larger response of the stabilization systems which is plausible for compensating additional friction torques.

V. Conclusion

In this contribution, parameter identification procedures as part of the commissioning process of a self-stabilizing monorail vehicle were discussed. The proposed procedures in time and frequency domain allows the estimation of mechanical parameters that are required for the vertical stabilization and usually can only be roughly estimated from CAD data. Especially the presented time domain methods need only a simple excitation signal and can therefore be easily integrated into an overall automatic commissioning procedure. The plausibility of estimated parameters was compared, analyzed and confirmed in various procedures. Further on the parameter values were used for the control of the real vehicle. Various dynamic and static disturbances were tested by which the stability and robustness of the system was confirmed. In further work the proposed procedures will be experimentally evaluated with other vehicle configurations (e. g. different cabins).

Acknowledgment

This contribution is accomplished within the research project MONOCAB OWL funded by the European Regional Development Fund (ERDF) and the Ministry for Transport of the state of North-Rhine Westphalia (Germany).

The conceptual idea of the MONOCAB originates from Landeseisenbahn Lippe e.V. whose approach was awarded with the German Mobility Award 2018.

References

[1] C. Moffett, "The Edge of the Future in Science. Transportation and the Gyroscope - Louis Brennan's Mono-Rail Car," *McClure's Magazine*, vol. 30, pp. 163–173, 1907. [Online]. Available: http://www.catskillarchive.com/rrextra/odgyro.Html

[2] A. Scherl, *Ein neues Schnellbahn-System: Vorschläge zur Verbesserung des Personen-Verkehrs von August Scherl*. August Scherl, 1909.

[3] P. P. Schilovsky, *The Gyroscope: Its Practical Construction and Application, Treating of the Physics and Experimental Mechanics of the Gyroscope, and Explaining the Method of Its Application to the Stabilization of Monorailways, Ships, Aeroplanes, Marine Guns, Etc.* Spon, 1924.

[4] C. J. Heiberg, D. Bailey, and B. Wie, "Precision spacecraft pointing using single-gimbal control moment gyroscopes with disturbance," *Journal of Guidance, Control, and Dynamics*, vol. 23, no. 1, pp. 77–85, 2000.

[5] A. Giallanza and T. Elms, "Interactive roll stabilization comparative analysis for large yacht: gyroscope versus active fins," *International Journal on Interactive Design and Manufacturing (IJIDeM)*, vol. 14, no. 1, pp. 143–151, 2020.

[6] K. Iuchi, H. Niki, and T. Murakami, "Attitude control of bicycle motion by steering angle and variable cog control," in *31st Annual Conference of IEEE Industrial Electronics Society, 2005. IECON 2005.* IEEE, 2005, pp. 6–pp.

[7] L. Keo and M. Yamakita, "Control of an autonomous electric bicycle with both steering and balancer controls," *Advanced Robotics*, vol. 25, no. 1-2, pp. 1–22, 2011. [Online]. Available: https://doi.org/10.1163/016918610X538462

[8] P. Y. Lam, "Gyroscopic stabilization of a kid-size bicycle," in *2011 IEEE 5th International Conference on Cybernetics and Intelligent Systems (CIS)*. IEEE, 2011, pp. 247–252.

[9] J. Kooijman and A. Schwab, "A review on bicycle and motorcycle rider control with a perspective on handling qualities," *Vehicle System Dynamics*, vol. 51, no. 11, pp. 1722–1764, 2013. [Online]. Available: https://doi.org/10.1080/00423114.2013.824990

[10] H. Yetkin, S. Kalouche, M. Vernier, G. Colvin, K. Redmill, and U. Ozguner, "Gyroscopic stabilization of an unmanned bicycle," in *2014 American Control Conference*. IEEE, 2014, pp. 4549–4554.

[11] C.-F. Huang, Y.-C. Tung, and T.-J. Yeh, "Balancing control of a robot bicycle with uncertain center of gravity," in *2017 IEEE International Conference on Robotics and Automation (ICRA)*, 2017, pp. 5858–5863.

[12] D. Lemus, A. Berry, S. Jabeen, C. Jayaraman, K. Hohl, F. C. van der Helm, A. Jayaraman, and H. Vallery, "Controller synthesis and clinical exploration of wearable gyroscopic actuators to support human balance," *Scientific reports*, vol. 10, no. 1, pp. 1–15, 2020.

[13] N. C. Townsend and R. A. Shenoi, "Gyrostabilizer vehicular technology," *Applied Mechanics Reviews*, vol. 64, no. 1, 2011.

[14] M. Griese, F. Kottmeier, and T. Schulte, "Vertical control of a self-stabilizing monorail vehicle," in *IECON 2021–47th Annual Conference of the IEEE Industrial Electronics Society*. IEEE, 2021, pp. 1–6.

[15] M. Griese, S. D. Mousavi, and T. Schulte, "Modeling the vertical dynamics of a self-stabilizing monorail vehicle," in *2021 9th International Conference on Control, Mechatronics and Automation (ICCMA)*. IEEE, 2021, pp. 205–210.

[16] ——, "Hil simulation of a self-stabilizing monorail vehicle," in *IECON 2022 – 48th Annual Conference of the IEEE Industrial Electronics Society*, 2022, pp. 1–6.

[17] R. Isermann and M. Münchhof, *Identification of dynamic systems: an introduction with applications*. Springer, 2011, vol. 85.

[18] H. Ahmed and M. Tahir, "Accurate attitude estimation of a moving land vehicle using low-cost mems imu sensors," *IEEE Transactions on Intelligent Transportation Systems*, vol. 18, no. 7, pp. 1723–1739, 2016.

[19] J. Lagarias, J. Reeds, M. Wright, and P. Wright, "Convergence properties of the nelder–mead simplex method in low dimensions," *SIAM Journal on Optimization*, vol. 9, no. 1, pp. 112–147, 1998. [Online]. Available: https://doi.org/10.1137/S1052623496303470

[20] P. Welch, "The use of fast fourier transform for the estimation of power spectra: A method based on time averaging over short, modified periodograms," *IEEE Transactions on Audio and Electroacoustics*, vol. 15, no. 2, pp. 70–73, 1967.

[21] R. Pintelon and J. Schoukens, *System identification: a frequency domain approach*. John Wiley & Sons, 2012.

[22] M. W. Jeffrey, "Introduction econometrics a modern approach 5th ed," 2009.